Wood Sci. Technol. 16: 35–58 (1982)

Wood Science and Technology

© Springer-Verlag 1982

Acoustic Emission from Softwoods in Tension

M. P. Ansell

School of Materials Science, University of Bath, Claverton Down, Bath, England *

Summary. Acoustic emission (AE) monitoring is a non-destructive testing technique widely used to detect flaw development and crack propagation in metals, ceramics, polymers and composite materials.

This paper relates the AE – strain characteristics from three softwoods tested in tension to mechanisms of deformation observed by scanning electron microscopy. All wood specimens are identical in size and radial-longitudinal in orientation, enabling the path of failure through planes of earlywood and latewood to be examined.

It is found that the proportion of earlywood to latewood in each species has a marked effect on the shape of the AE-strain curves. Parana pine, containing very few latewood tracheids, exhibits a close to linear relationship between log cumulative emissions and strain until close to failure when the count rate increases rapidly. Douglas-fir, which has well-defined earlywood-latewood boundaries generates many AEs at low strain and there is greater variation in the shape of the AE characteristic between samples.

Parana pine and Douglas-fir are tested at 20 °C (12.5 % EMC). Scots pine is also stressed at 20 °C (12.5 % EMC), 20 °C (0.7 % EMC) and 80 °C (0.7 % EMC), to assess the effect of moisture content on AE.

Values of Young's modulus, stress at failure and work of fracture for the three softwoods are compared with the AE-strain data. Although the work of fracture is related to the total AEs to failure, no direct proportionality exists between the two parameters.

Finally, the AE-strain data for plywood and glass-reinforced plastic (GRP), both man-made composite materials, are compared with those of wood, the natural composite material.

Introduction

Acoustic emission (AE) testing is a well-established technique whereby elastic stress waves generated by opening flaws and moving cracks in the bulk or on the surface of deforming materials are detected by a transducer mechanically driven by the waves. The electrical output from the transducer is amplified and can be processed in a number of ways by ancillary electronic equipment, depending on the amplitude and rate of generation of stress waves and the desired way of presenting data. The technique of

* S.R.C. support for this work under grant No. GR/A/13257 is gratefully acknowledged. The support of Professor Bryan Harris of the School of Materials Science, University of Bath and Dr. J. M. Dinwoodie of the Building Research Establishment, Princes Risborough is greatly appreciated. Mr. B. Dobraszczyk performed the impact tests.

0043-7719/82/0016/0035/$ 4.60

ring-down counting, where rising electrical pulses which exceed a given threshold voltage are counted as individual events, is adopted in this work.

The value of stress wave detection in materials testing lies in the ability to monitor the initiation and growth of flaws in progressively strained or fatigued material. In a test to failure cracks are allowed to propagate through the sample. In a non-destructive test only a proportion of the failure stress is applied. The rate of flaw extension depends on the material type, the density of flaws, the position of micro- and macro-interfaces and environmental influences such as temperature, humidity and the nature of the applied stress. AE-strain characteristics provide an insight into the structural integrity of a material throughout the duration of a mechanical test, which can be related to physical properties such as the modulus of elasticity, (MOE), stress at failure and work of fracture or toughness.

Many papers describing AE from materials other than wood may be found in the literature. Birchon (1975) explains the success of AE testing compared with other non-destructive testing techniques. Two ASTM (1972 and 1975) publications describe the principles and applications of AE detection in a number of materials. Recent industrial applications are described in a review paper by Arrington (1978) who includes references to work involving metals, ceramics and other materials.

The analysis of AEs from fibre-reinforced composite materials is reviewed by Guild et al. (1976). Other significant papers on reinforced plastics have been published by Fuwa et al. (1975, 1976), Becht et al. (1976) and Sims et al. (1977).

Pilots of wooden aircraft and gliders have been aware of the creaking of their airframes, probably due to friction at joints. More importantly, miners know that the creaking of pit-props is a warning of their imminent failure. However the first literature reference to detection of stress waves from wood and indeed from other materials, is attributed to Kaiser (1950). His observation of the irreversibility of AE from many materials cycled under load is now generally known as the Kaiser effect.

Miller (1963) detected sound emissions from wood using a microphone but it was Porter (1964) who first used a piezo-electric crystal, in conjunction with an amplifier, high pass filter and an electronic counter in a study of emissions from wood cleavage specimens. In a joint paper, (Debaise et al. 1966), he and co-authors investigated flaw growth in western white pine. The softwood was stressed in the open cleavage and static bending modes and by tension parallel and compression parallel to the grain modes. It was concluded that in tension, bending and cleavage, AE resulted from "flaw growth proceeding unstably for short flaw extensions" and that this growth was activated at low average strain levels. In compression applied loads closed intrinsic flaws, with few emissions as a consequence. The heterogeneous structure of wood was stated to be of major importance to the pattern of flaw development.

AE from 50 in. beams of 2 in. by 4 in. Douglas-fir, western Hemlock and western red cedar timber stressed by three point bending is described by Adams (1969). A piezo-electric accelerometer was used as detector, operating between 200 Hz and 10 kHz. At the proportional limit a marked increase in count rate was found with the onset of micro-failure development. The presence of knots affected the micro-failure

pattern, possibly "due to drying checks formed in and around them". Count-deflection curves led to no precise estimate of the failure stress. The detection of AEs from wooden beams in large scale constructions was also mentioned by Muenow (1971, 1972).

Porter et al. (1972) used AEs to predict the ultimate bending strength of 2 in. by 6 in. Douglas-fir finger joints. By obtaining AE data at a load level just beyond the proportional limit a ± 10% accuracy in estimating fracture loads was found to be possible.

Most recently Ansell (1978) detected AEs from Scots pine wood tested in tension. The wood was stressed at two levels of equilibrium moisture content (EMC) and with grain angles of 0°, 15°, 30° and 45°. The change in the mechanisms of tensile deformation with increase in grain angle from 0° to 45° were reflected in the shape of the AE-strain curves and total emissions to failure.

This paper compares flaw development and structural deformation in three softwoods, plywood and glass-reinforced plastic (GRP) tested in tension to failure. AEs monitor the progress of flaw growth throughout the test and scanning electron microscopy reveals the mechanisms of deformation and paths of failure in these materials.

Values of MOE, failure stress and work of fracture are compared for the three softwoods and correlation between AE and these parameters is discussed. Scots pine (*Pinus sylvestris*), Douglas-fir (*Pseudotsuga taxifolia*) and Parana pine (*Araucaria angustifolia*) are tested at 20 °C and 12.5% EMC. The effect of moisture content on fracture and AE output is also investigated for Scots pine. The AE behaviour of plywood and GRP in tension and mechanisms of structural deformation are compared with wood.

Sample Preparation

Scots pine wood was obtained from a 60 year old tree felled in the Forest of Dean in Wales. Trunk sections of approximately 45 cm in diameter were sawn into 2 cm width planks along the tree axis and these were kiln-dried and seasoned at the Building Research Establishment, Princes Risborough to 65% r.h. at 20 °C. Similarly seasoned Douglas-fir and Parana pine was obtained from the BRE. Clear wood was selected, free of knots, resin bands, compression wood and heartwood.

Samples were cut with the radial-longitudinal orientation and dimensions shown in Fig. 1. The dimensions were achieved by rough cutting followed by sanding in metal jigs. Plywood samples were cut to the same dimensions. The 7-ply wood was 1 cm in board thickness, identical to the wood sample width. 2.5 mm sections were prepared from the board so that 3 plies were aligned with the wood cells parallel to the specimen direction and 4 plies with the cell direction aligned perpendicularly. The major contribution to strength was thus made by the 3 plies with tracheids parallel to the sample length.

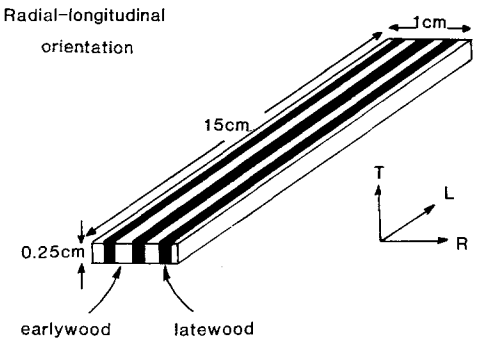

Fig. 1. Specimen orientation and dimensions

Commercially manufactured GRP samples were cut to 15 cm in length and 1 cm in width from a sheet of 1.4 mm in thickness. Glass fibres, cross-woven at right angles in an epoxy resin matrix, were aligned at 0° and 90° to the sample length.

Abraded aluminium tabs of 1.5 cm x 2.5 cm in surface dimension and 1.65 mm thick were glued with epoxy resin to the ends of the samples. A clear 10 cm length of sample was exposed between the tabs. The space between the overlapping edges of the tabs was filled with epoxy resin.

All specimens were tested in tension in an Instron 1121 machine with a constant cross-head speed of 0.1 mm/min. The serrated jaws of the Instron grips (Fig. 2) were tightened manually, biting into the softer aluminium tabs so that there was no possibility of shear between the aluminium tabs and the jaws. The rigid epoxy resin

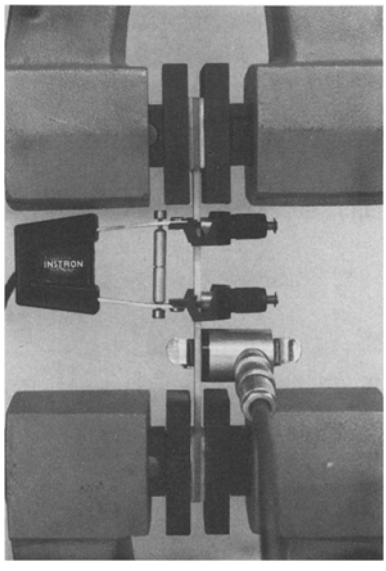

Fig. 2. Specimen held in Instron grips

between the tab edges prevented lateral compression of the wood which would otherwise have lead to premature failure in the wood close to the tabs and the generation of spurious AEs. An Instron extensometer was clipped to the sample to measure strain (Fig. 2).

Acoustic Emission Apparatus

Flaw growth or failure within samples stressed in tension released energy in the form of AEs. These AEs propagated through the wood and were detected by a PZT-5 (lead zirconate-titanate) piezo-electric transducer (Fig. 2), coupled firmly to the specimen with silicone grease. This acoustic bond had no effect on the mechanical properties of the wood but was essential to avoid loss of acoustic signal at the transducer-sample interface.

Dunegan 3000 series equipment was used to amplify and process the detected signals. A flow diagram (Fig. 3) illustrates the inter-relationship between applied load, measured strain and acoustic signals in the experimental set up. An S/D-60P pre-amplifier boosted the signal from the transducer by 1,000x (60 dB) and contained a band pass filter which passed signals between 100 and 300 kHz. Thus low frequency electrical noise in the laboratory was eliminated and only acoustic signals between these frequencies, coinciding with the frequency range of efficient transducer operation, were passed for processing. A second amplifier was set with a gain of 10x, (20 dB), giving an overall gain of 10,000x, (80 dB). The data then consisted of variable frequency, variable amplitude voltage bursts, each containing cycles of gradually decaying amplitude (Fig. 4). Each rising positive signal of 100 μV greater amplitude was counted by a digital counter which after amplification accepted signals of greater than 1 Volt. An output was made to a DVM which displayed accumulated counts. This output related the AEs to the state of strain in the sample when correlated with

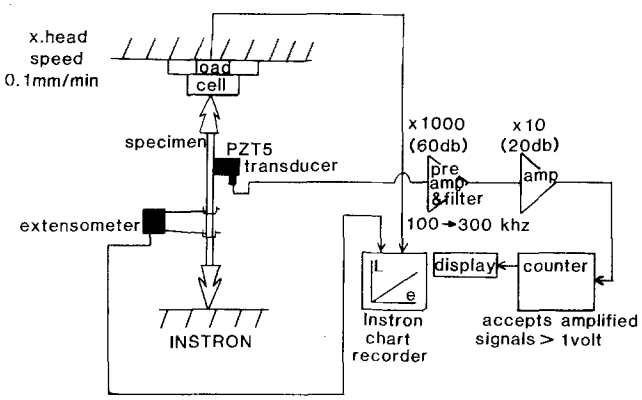

Fig. 3. Instron and acoustic emission system

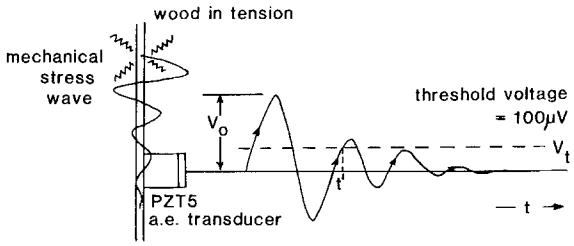

Fig. 4. Ring down signal

stress-strain information from the load cell and extensometer. Accumulated counts were recorded at equal intervals of extension (every 0.002 mm = ~0.01 % strain) and these values were plotted directly against strain.

Acoustic Emission Theory

It is not possible using the counting technique described above to assess the amplitude of individual stress waves. However large amplitude emissions result in many rising pulses crossing the pre-set threshold voltage and thus the number of pulses detected relates to the amplitude of the pulse. The relationship between strain energy dissipation in tensile-tested specimens and the number of rising pulses counted above a threshold voltage was examined by Harris et al. (1972). In Fig. 4, a mechanical stress wave, generated by energy release at a point in a wood sample, propagates along the sample, decaying in amplitude with distance. For simplicity, a single mechanical pulse from the decaying stress wave is considered to excite the piezo-electric transducer, which in turn generates an oscillating electrical signal, decaying in amplitude, of peak voltage V_o. Assuming exponential decay of this signal, the voltage at time, t, V_t, is expressed by:

$$V_t = V_o \exp(-\beta t) \sin \omega t \tag{1}$$

where V_o = initial peak voltage
β = damping constant
ω = angular frequency ($\omega = 2\pi\nu$).

The number of peaks counted above the threshold voltage,

$$N = \nu t' = \frac{\omega t'}{2\pi} \tag{2}$$

where t' is the time at which the last rising voltage peak crosses the threshold voltage. As the last peak counted is an integral number of wavelengths from the origin it is seen from Eq. (1) that:

$$V_{t'} = V_o \exp(-\beta t')$$

Therefore from Eq. (2):

$$N = \frac{\omega}{2\pi\beta} \ln \frac{V_o}{V_t} \tag{3}$$

Now assuming that the voltage V_o generated by the transducer is proportional to the square root of the energy, E, in the single mechanical pulse, from Eq. (3)

$$N \propto \ln V_o$$

and so in theory the number of counts:

$$N \propto \ln E \tag{4}$$

In practice this derived proportionality between the number of counts and the dissipated strain energy is far too simplistic. The transducer is only excited efficiently by pulses with frequencies close to the resonant frequency of the transducer. Furthermore the location of the sources of stress wave generation will vary with distance from the transducer. High frequency AEs will also be attenuated rapidly by inhomogeneities in wood and composite structures. Resonances may also be excited in the sample and in the transducer which will further invalidate the simple premise of Eq. (4).

When observing fracture geometries in a set of wood specimens considerable variations are seen. It could therefore be expected that AE-strain curves for these specimens might show little similarity. However, as will be seen in the reported results, the curves for sets of specimens tested in specific environments are, in fact, found to be remarkably similar in general trend. Most importantly the curves give an indication of how strain energy release depends on the state of sample strain.

By testing all samples with identical dimensions at the same strain rate, an excellent basis for comparing deformation behaviour to failure is achieved. The AE 'signature' thus provides detailed information on structural change throughout the duration of the test.

Experimental Results

Scots Pine 20 °C and 12.5 % EMC

The moisture content of the Scots pine wood was calculated by weighing a control set of seasoned wood samples in the testing laboratory, and then by drying the wood in an oven at 100 °C until constant weight was achieved.

The appearance of Pinus sylvestris sapwood is shown in the transverse section of Fig. 5. Notable features are the thin-walled earlywood cells with much smaller lumens. The average MOE for earlywood (5.1 GNm^{-2}) and latewood (17.1 GNm^{-2}) in Scots Pine were measured by Ansell (1978). Along radial rows of cells a gradation in the cell size is seen in latewood, whereas earlywood cells have fairly uniform dimensions. Ray cells pass uninterrupted from one annual ring to the next. The diffuse boundary

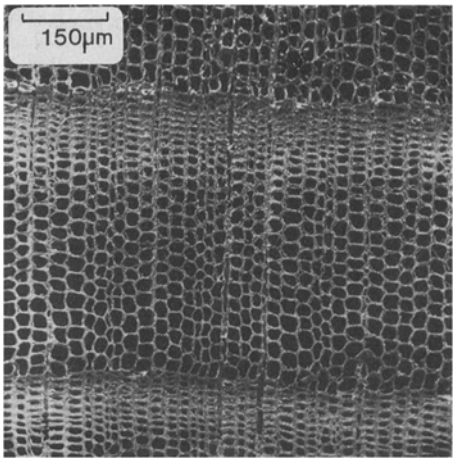

Fig. 5. Scots pine, transverse section

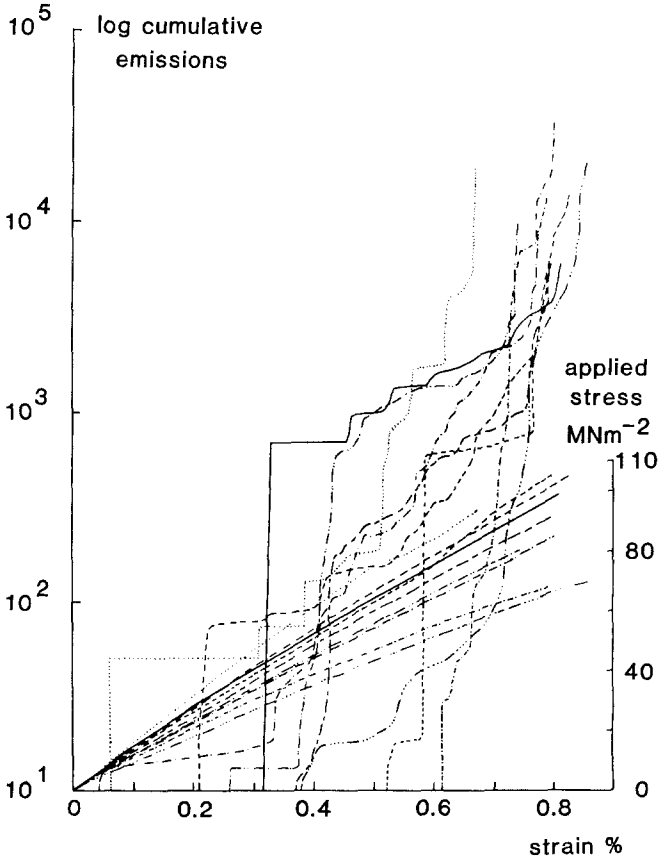

Fig. 6. Scots pine 20 °C, 12.5 % EMC

between spring and summer growth contrasts with the sharp summer-winter boundary at the outer edge of each annual ring. All these structural features influence fracture mechanisms and AE generation.

Stress-strain characteristics and AE-strain curves are co-plotted in Fig. 6. Each AE curve corresponds to a stress-strain curve according to the line coding. The rate of generation of AEs at small strains is usually low whereas close to failure the emission rate is high. By plotting AEs on a logarithmic scale a more detailed examination of stages in flaw development can thus be achieved by effectively amplifying the low strain end of the AE characteristic and compressing it at high strains. In all the data for wood there is some variation in the slope of the stress-strain curves, which individually are close to linear right up until failure. This spread is a function of the variations in the proportion of latewood to earlywood which will affect the elastic modulus of each specimen.

Referring to Fig. 6 it is seen that nearly all nine samples fail within $0.8 \pm 0.1\,\%$ strain. The total AEs to failure are also fairly close, although the shape of the individual characteristics is variable, indicating a non-uniform rate of flaw growth. The AE curves are a combination of sharp vertical increases interspersed with more gradual accumulations of counts.

Slow count rates are attributed to gradual opening of microflaws as the helically-wound cellulose cell wall reinforcement extends elastically within the matrix of hemi-

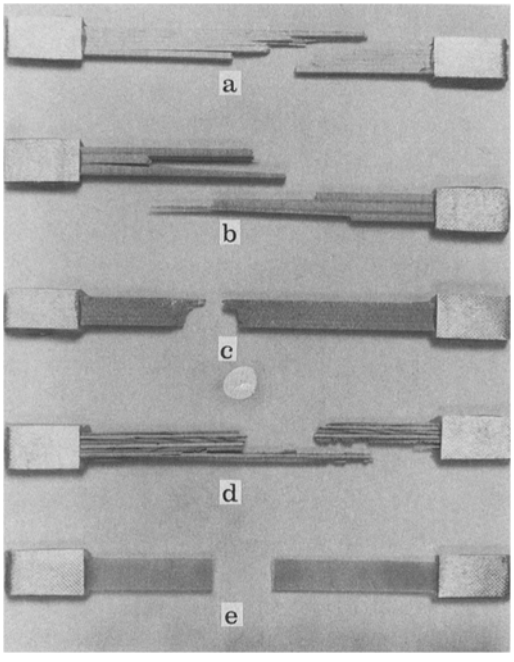

Fig. 7. Fractured specimens: **a** Scots pine; **b** Douglas-fir; **c** Parana pine; **d** plywood. E 0°–90° GRP

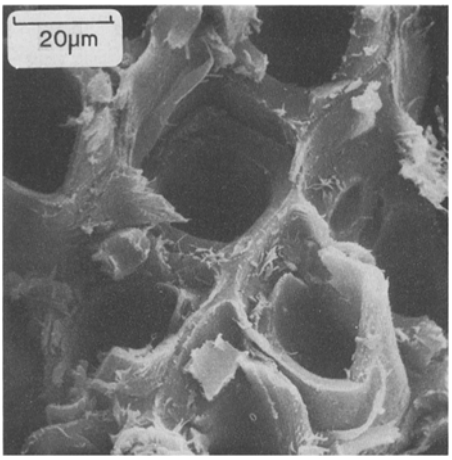

Fig. 8. Brittle failure in Scots pine latewood

cellulose and lignin. The rapid increases in AE are assigned to either interlaminar shear in planes of weakness, for example at ray cell-tracheid interfaces and earlywood – latewood interfaces, or to brittle failure of tracheids, both of which are fast failure events.

Representative fractured specimens for all materials described in this paper are photographed in Fig. 7. The line of crack propagation in Scots pine is seen to pass either along the interface between earlywood and latewood in the direction of cell growth, or transversely, perpendicular to the cell axis.

Scanning electron micrographs reveal mechanisms of cell extension and failure. The Scots pine latewood tracheids of Fig. 8 have fractured in an essentially brittle way. The crack has propagated rapidly through the interlamellar material and primary and secondary wall layers. The many cellular interfaces and the annual ring macrostructure in wood inhibit catastrophic crack propagation until a sufficiently large stress concentration has built up. Usually a rapidly accelerating crack passes through the specimen, instantaneously, along the path of greatest weakness, and no deviation from linearity is thus seen in the stress-strain curve, (Fig. 6). Shear between latewood cells (Fig. 9) often occurs where planes of ray cells interact with the longitudinal tracheids. In this case the shear is intercellular. The S_2 cell wall layer of longitudinally-stressed tracheids will tend to unwind and this trend can occasionally be observed (Fig. 10). Here the right-handed spiral of the S_2 microfibrils is clearly seen, indicating that micro-flaws were developing along the helical windings prior to cell fracture. Finally Fig. 11 illustrates the effect of latewood-earlywood interfaces in arresting the progress of major cracks in Scots pine. The crack passing transversely across earlywood cells has been diverted parallel to the adjacent latewood cells.

Referring to Fig. 6 it is seen that the many possible fracture paths result in variations in the shape of AE curves. However, failure strains and total counts to failure are close, suggesting similar fracture energies.

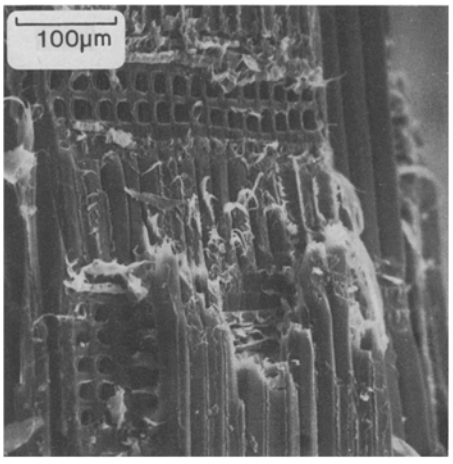

Fig. 9. Shear in Scots pine latewood

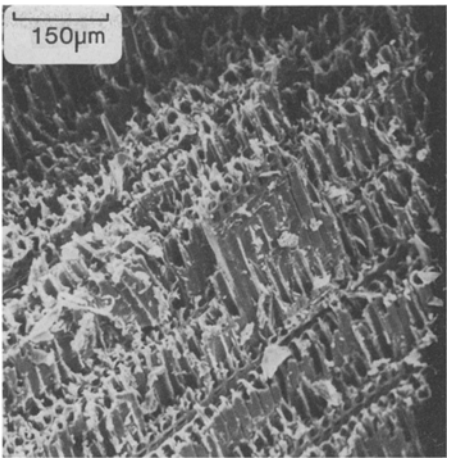

Fig. 10. Helically-unwound Scots pine tracheids

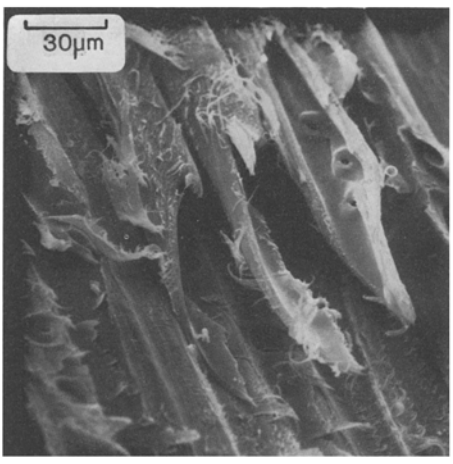

Fig. 11. Fractured Scots pine, earlywood-latewood interface

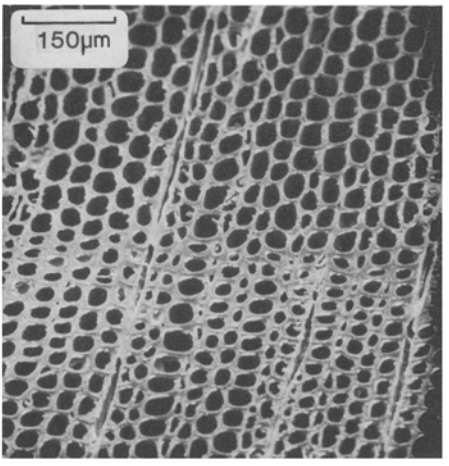

Fig. 12. Parana pine transverse section

Parana Pine 20 °C and 12.5 % EMC

The cellular structure of this softwood, Fig. 12, imported from South America, is determined by the uniform climate in which it is grown. Very little latewood is evident in the micrograph of a transverse section. Only a few cell widths of thicker latewood cells divide two regions of earlywood. Thus the overall structure of clear Parana pine sapwood is very simple, consisting principally of earlywood tracheids and ray cells.

The AE response (Fig. 13) from specimens pulled in tension reflects this structural uniformity. Seven out of nine characteristics fall within a narrow envelope and an approximately log-linear relationship exists between cumulative emissions and strain.

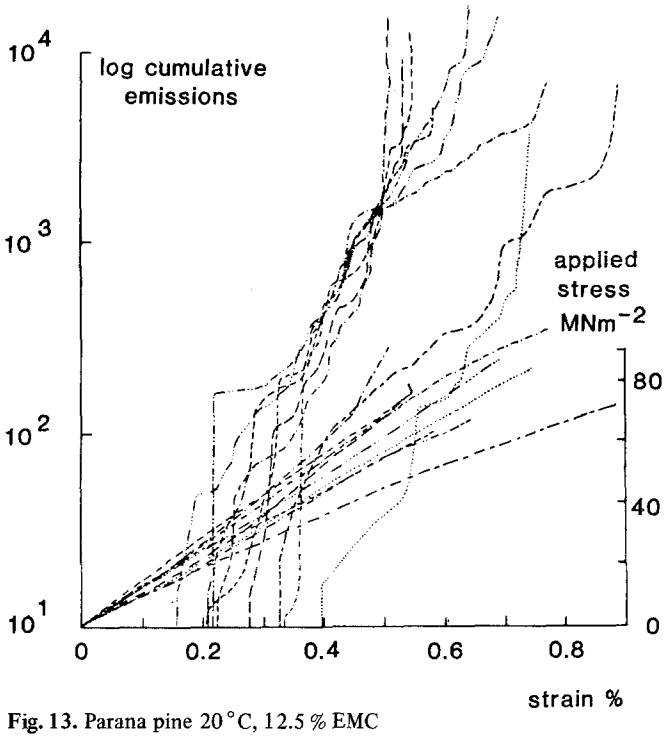

Fig. 13. Parana pine 20 °C, 12.5 % EMC

The usual upturn in the characteristic occurs at failure. The stress-strain curves are close to linear with some variation at high strains.

Figures 7 and 14 demonstrate the smooth appearance of the fracture surface of Parana pine. In the micrograph of radial-longitudinal planes of cells, the progress of the propagating crack has been checked by ray cells. A combination of shear, at the

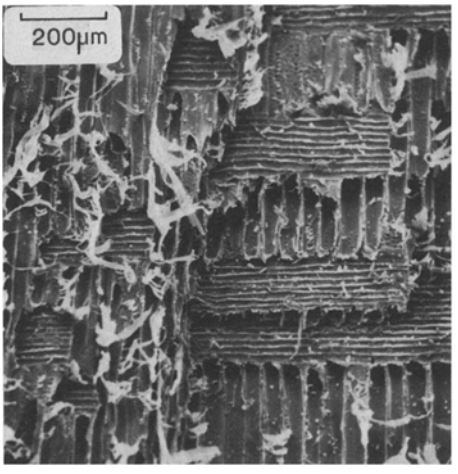

Fig. 14. Fractured Parana pine

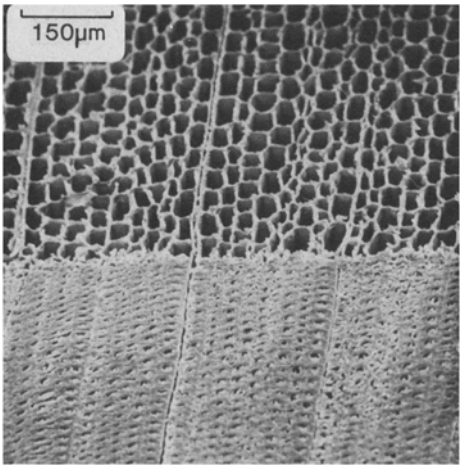

Fig. 15. Douglas-fir, transverse section

ray cell planes, and brittle fracture across cells, eventually leads to fracture. Flaw development during the tensile test is a bulk process and the fracture surface only epitomizes the planes of weakness present throughout the wood sample. In conclusion, tensile stressing of the uniformly structured Parana pine leads to smooth fractures and progressive emission of stress waves.

Douglas Fir, 20 °C and 12.5 % EMC

The transverse section of Douglas-fir (Fig. 15) discloses the considerable difference in the dimensions of earlywood and latewood tracheids. The AE curves of Fig. 16 contrast strongly with Figs. 6 and 13 for Scots pine and Parana pine. Nearly all samples begin to emit at less than 0.2 % strain. Generally, rapid initial emission rates are followed by a period of more controlled emission until the usual upturn in the emission curve is reached at the failure stress. There is however considerable scatter in the

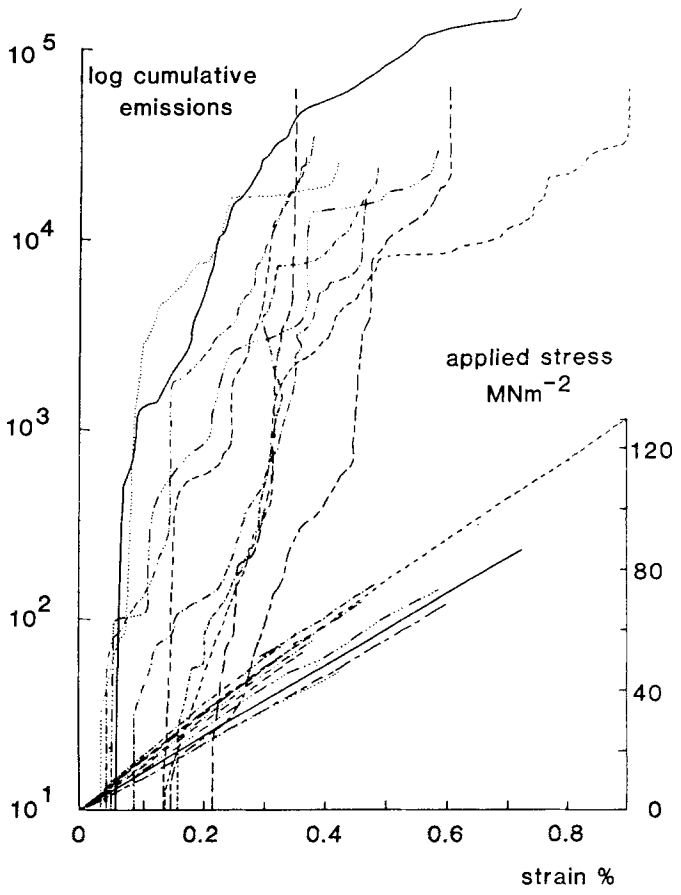

Fig. 16. Douglas-fir 20 °C, 12.5 % EMC

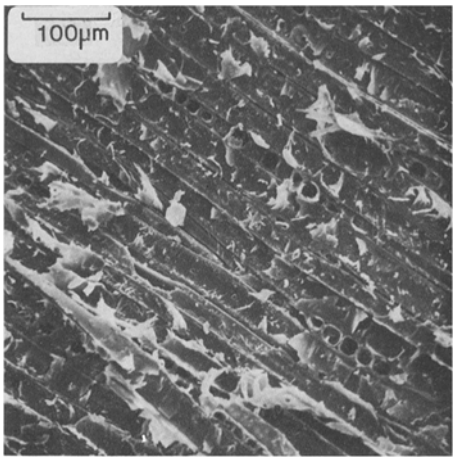

Fig. 17. Shear failure in Douglas-fir

values of failure strain although the total number of emissions to failure is fairly constant.

An electron micrograph (Fig. 17) displays a frequently observed plane of intracellular shear at the earlywood-latewood interface in Douglas-fir. The debris of earlywood cells adheres to latewood cells lying in the tangential longitudinal plane. Ray cells are clearly visible in cross-section. It is suggested that the rapid initial accumulation of counts (Fig. 16) results from interfacial shear between planes of earlywood and latewood of different stiffness and from the movement of flaws in the seasoned wood. Thereafter AEs accumulate more gradually as the wood cells deform elastically. Irreversible flaw growth in cell walls leads to the build up of high stress concentrations. Close to failure cracks swiftly propagate from these points leading to complete or partial fracture. The associated instantaneous burst of stress waves is the result of brittle fracture and fast shear which cause the breaking wood to reverberate.

Toughness, Stiffness and Acoustic Emission

Specimens of three softwood species identical in dimensions, have been tested in tension to failure. The stress-strain curves show close to Hookean behaviour right up until failure. Load cycling specimens to approximate 90% of their failure stress causes little deviation from this initial linearity. A value for the Young's modulus (MOE) can be calculated from the average slope of the stress-strain curve. Average values for failure stress, failure strain and the MOE, including the standard deviation for each parameter are listed in Table 1 for the three softwoods.

Apart from the MOE another important material parameter is the toughness, or resistance to the propagation of cracks. The measurement of work of fracture by Charpy impact testing is a convenient way of comparing the toughness of materials.

Table 1. Properties of three softwoods with radial-longitudinal orientation. Results for each species are the average for nine samples with the standard deviation in brackets

Material	Failure stress	Failure strain	Modulus of elasticity	Total counts at failure	Work of fracture	Density
	MNm^{-2}	%	GNm^{-2}	k counts	kJm^{-2}	kgm^{-3}
Scots pine	85.4 (16.0)	0.76 (0.10)	11.3 (1.88)	14.6 (8.6)	23.0 (4.1)	505
Parana pine	80.1 (11.2)	0.70 (0.13)	12.0 (3.01)	9.9 (5.2)	16.7 (2.7)	498
Douglas-fir	70.3 (23.0)	0.53 (0.17)	13.4 (1.92)	38.5 (19.5)	24.1 (3.2)	543

The orientation and dimensions of notched wooden Charpy specimens are shown in Fig. 18. The grain of the wood is aligned so that a crack developing from the root of the notch has to pass through several annual rings, just as the crack in tensile specimens has to pass through bands of earlywood and latewood. The values of work of fracture are listed in Table 1. They are greater than $10^4 Jm^{-2}$ classifying wood as a tough material.

Traditional tough materials, such as steel, derive their toughness from their ability to yield in a ductile manner after initial Hookean behaviour. Wood, however, has a close to linear stress-strain curve right up to failure just like crack-sensitive materials such as glasses and ceramics. Furthermore the appearance of fractured wood is often jagged (Fig. 7) and the microstructure appears brittle (Fig. 8). However, the intricate helically wound cellulose reinforcement in the wood cell wall allows considerable elastic deformation under high applied stresses, and a great deal of work is done in deforming the fibre-matrix interfaces throughout the bulk of a stressed wood sample. Even after partial fracture of a sample has occurred, bands of earlywood and latewood inhibit further progress of the crack until a sufficiently high crack-initiating stress concentration has again built up.

The parameters recorded in Table 1, including total counts to failure, are now examined in order to assess any relationship between stiffness, toughness, total AEs at failure and the annual ring definition in each softwood species. Taking each species individually the following observations can be made.

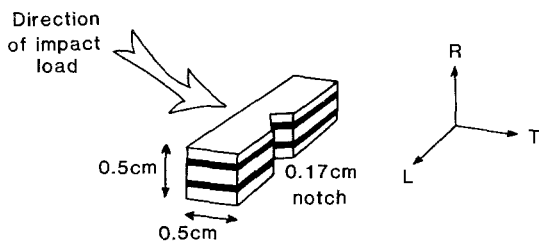

Fig. 18. Charpy pendulum impact test

Scots pine fails at the highest values of stress and strain and has the lowest stiffness of the three softwoods. The total counts to failure are intermediate in number between the total for Parana pine and Douglas-fir. The annual rings are less well-defined than in Douglas-fir but are obviously more easily distinguished than those in Parana pine. The toughness is close to the value for Douglas-fir.

Parana pine fails at intermediate values of stress and strain and has an intermediate value of stiffness. AEs at failure are by far the lowest and the toughness is significantly the lowest too. Annual rings are almost non-existent.

The lowest values of failure stress and strain are recorded for Douglas-fir, but this wood is marginally the stiffest. The total AEs to failure are by far the highest and the annual rings are very well defined. The work of fracture is close to that for Scots pine.

Thus the following relationships are seen:

1. Stiffer materials fail at lower stresses and strains, implying that stiffer material is more brittle.

2. The sharpness of definition of the annual rings correlates with the total AEs at failure. Thus the greater the difference in properties between earlywood and latewood, i.e. wall thickness, lumen size, number of cells per annual ring width, and the better delineated the annual ring interfaces are, then the more AEs can be expected.

3. There is an order correlation between the material toughness and the AEs to failure, but not a proportional one, as predicted by the earlier analysis.

Deriving the specific parameters, by dividing each parameter by the wood density, (Table 1), does not significantly alter the parameter rankings.

In all softwoods toughness is attributed to the helically-wound tracheids and intercellular interfaces which resist crack propagation, but in the case of Douglas-fir the earlywood-latewood boundaries appear to make an extra contribution to the overall material toughness.

Glass-Reinforced Plastics

It is instructive to compare the AE output from GRP in tension with those from wood. The GRP was prepared, as described earlier, with glass fibres aligned at 0° and 90° to the axis of the test piece. Glass fibres, 50% by volume, are woven in strands and held in a matrix of epoxy resin.

The stress-strain and AE-strain curves appear in Fig. 19. Although the average modulus of elasticity ($\sim$20 GNm^{-2}) and fracture strain ($\sim$1.2%) are somewhat higher than those for wood, these values are similar enough for the AE characteristics to be compared. As might be expected for tensile specimens cut from a uniform sheet of synthetic material the stress-strain curves are very close together and smooth in shape. Furthermore, the AE-strain curves all have the same general shape. AEs begin to accumulate at about 0.15% strain, building up smoothly until failure when the usual rapid increase in AEs is noted.

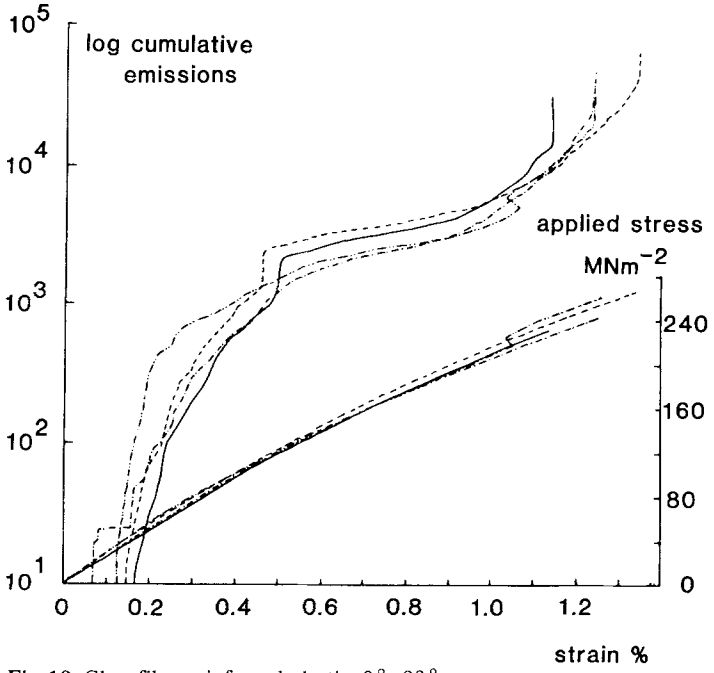

Fig. 19. Glass fibre reinforced plastic, 0°–90°

GRP deforms rather differently to wood. Initially the load is carried mainly by the fibres but as the weakest brittle fibres fail, work is done in debonding these fibres and subsequently in pulling them out from the matrix. As a result of the regular arrangement of fibres in the resin matrix, the AE curves are smooth and progressive in shape. Failure of the GRP, a fast, brittle event, is accompanied by a rapid burst of emissions as in wood.

The scale of the woven glass fibre reinforcement (~ 5 μm diameter) in GRP is very different to the helically-wound microfibrils in GRP (~ 150 Å in diameter). However the uniform AE-strain curves of GRP are more akin to those of Parana pine (Fig. 13) than to those of Scots pine and Douglas Fir (Figs. 6 and 16). Hence there is further support for the argument that the crack-stopping macro-interfaces represented by the earlywood and latewood in the latter two species, and the difference in the dimensions of the tracheids, contribute to the more erratic emission of stress waves. Unfortunately the thin sheets of GRP did not allow an estimation of the work of fracture by impact testing, but similar values to those for wood are expected.

Scots Pine at 20 °C and 80 °C with 0.7% EMC

The moisture content of wood directly affects its mechanical properties, (Bodig 1978). The AE characteristics for Scots Pine with an EMC of 0.7% were obtained at both 20 °C and 80 °C in order to gauge the effect of moisture and temperature. For the

tests at 80 °C the samples were heated in a temperature enclosure mounted on the Instron machine. Tests proceeded when constant sample weight was measured. The EMC was calculated by comparing specimen weight with oven dry weight from a control set of samples. Remarkable consistency was achieved. At 20 °C and approximately 0.7% EMC the tensile specimens were heated as before, cooled in a desiccator to 20 °C and subsequently tested in a flushed atmosphere of dry nitrogen.

The characteristics for Scots pine at 80 °C are seen in Fig. 20. The average failure stress is 46.1 MNm^{-2}, the average failure strain 0.33% and the average MOE is 13.9 GNm^{-2}. Thus the average stiffness of the 0.7% EMC wood is higher than for the 12.5% EMC wood (11.3 GNm^{-2}) whereas the failure stress and strain are considerably less. The AE-strain curves at 0.7% EMC are abrupt and close to vertical, differing radically from the more progressive curves seen in Fig. 6, at 12.5% EMC and 20 °C. Once a sufficiently high stress concentration has built up in the elastically deforming dry wood, rapid crack propagation occurs across the planes of earlywood and latewood and the failure surface is as a result far less jagged than the 20 °C material with a 12.5% equilibrium moisture content. There is a rather large variation in the strain at failure which is attributed to different rates of development of critical stress concentrations, a function, probably, of the surface and interfacial morphology.

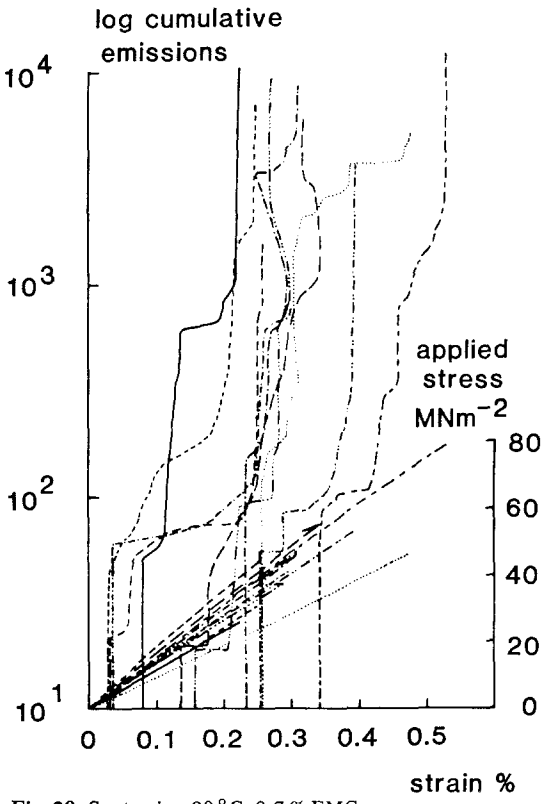

Fig. 20. Scots pine 80 °C, 0.7% EMC

On testing the dried wood at 20 °C the stress-strain and AE-strain curves of Fig. 21 are derived. The average failure stress is 48.2 MNm^{-2}, the average failure strain 0.39% and the average MOE is 12.3 GNm^{-2}. These values, compared with those at 20 °C and 12.5% EMC and those at 80 °C and 0.7% EMC, suggest that a little re-absorption of moisture took place during the test period. Nevertheless the AE-strain curves of Fig. 21 are very similar to those of Fig. 20, demonstrating the important effect of moisture on wood stiffness and flaw growth.

Charpy specimens of 0.7% EMC Scots pine were prepared as before and tested at 80 °C. A wide range of values of work of fracture was measured, too wide to be reported as useful data. This unpredictable behaviour does however correspond to the variations in AE output with respect to strain. Total AEs to failure averaged 7.3 k counts, half the average for Scots pine at 20 °C. At 12.5% EMC the cell wall can behave more elastically allowing potential stress concentrations to relax before they become critical, and toughness is as a consequence higher.

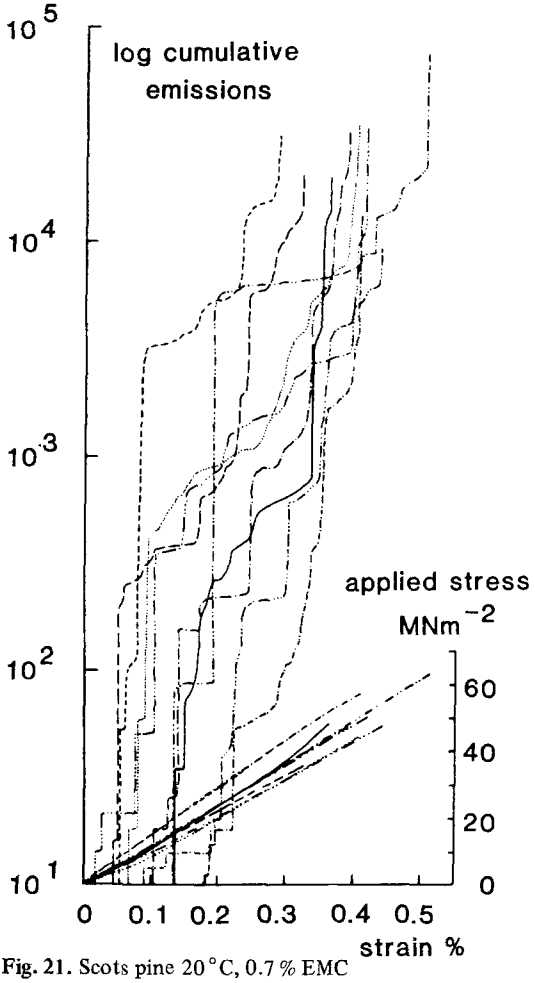

Fig. 21. Scots pine 20 °C, 0.7 % EMC

Finally, dried wood was allowed to regain moisture by leaving it for five days in the laboratory when constant weight was achieved. AE-strain curves for these samples are very similar to those in Fig. 6 for seasoned Scots pine, confirming the importance of EMC on wood properties.

Plywood 20 °C and 12.5 % EMC

Plywood has a laminated structure composed of layers of wood veneer with the cell directions alternately opposed at 90 ° to each other. The uniform laminated layers effectively model the earlywood and latewood planes seen in Scots pine and Douglas-fir, yet the layers are identical in thickness and parallel sided unlike the equivalent layers in natural wood.

Inspection of sectioned plywood by scanning electron microscopy (Fig. 22), reveals the cellular elements which make up plywood. In the lower half of the micrograph a radial section through one ply cuts across both earlywood and latewood cells. In the upper half a longitudinal section is seen in the adjacent ply. The glue which bonds the two plies together does not appear to penetrate more than one cell thickness on either side of the glue line. Five samples consisting of three strong plies and four weak ones, were tested and a typical fracture is seen in Fig. 7.

The usual curves are plotted in Fig. 23. There is some scatter in the shape of the stress-strain curves with an average MOE of 7.80 GNm^{-2}. The AE curves are very uniform with some variation at 0.4 % strain. The three samples which increase their count rate at 0.4 % strain before emitting more smoothly to failure, are samples in which one of the three strong plies failed prematurely, transferring the load to the other two plies. In the other two samples the three strong plies sustained the applied load right up until failure.

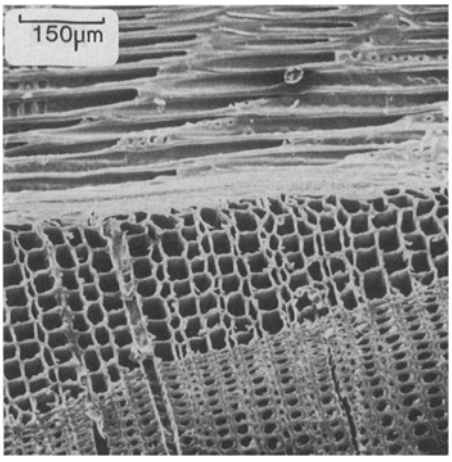

Fig. 22. Plywood transverse section

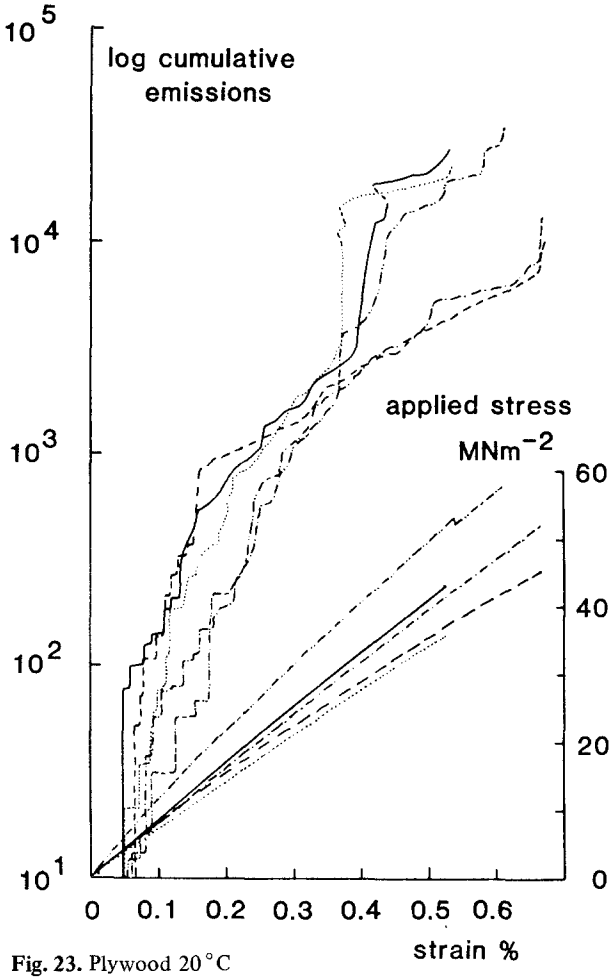

Fig. 23. Plywood 20 °C

Here in a 'model' wood system it is suggested that the AE at low strains is the result of progressive low energy deformation in the weak plies as seen in the ruptured plywood sample of Fig. 7. At failure the sharply rising AEs are due to irreversible deformation in the strong plies. For plywood the state of strain is reasonably proportional to the total counts at any stage in the tensile test. Reasonably reproducible AE-strain curves for plywood, compared with the wider scatter in Douglas-fir, are seen to be a function of the uniform laminated structure and the weakness of the layers of cells aligned at 90 ° to the direction of applied stress.

Conclusions

Important factors which contribute to mechanical properties of wood are the orientation of helically-wound cellulose microfibrils in the tracheid walls, the arrangement of

tracheids into bands of earlywood and latewood and the moisture content of the wood.

AE monitoring has been successfully utilised to record the stages of energy release in three softwoods tested in tension to failure. The form of the AE-strain curves is related directly to their annual ring structure, and the total AEs recorded at failure have an order correlation with toughness measured in impact.

In applications where a tough material with uniform properties is required, synthetic composites, such as GRP, and cross-laminated plywood deform in tension to failure in a more predictable manner, as reflected in their smoother AE-strain characteristics. AE testing is proposed as an excellent method for assessing the effect of structure and moisture content on the mechanical properties and failure mechanisms of wood. It may also be used in future to understand the effect on the properties of wood of creep, fatigue and exposure to adverse environments.

References

Adams, R. D. 1969: Fracture development in wood resulting from bending stresses and detected using the acoustic emission phenomenon. Masters Thesis. Department of Forestry, University of British Columbia

Ansell, M. P. 1978: Acoustic emission as a technique for monitoring fracture processes in wood. Proceedings of symposium: Structural use of wood in adverse environments. Vancouver, B.C.

Arrington, M. 1978: Some industrial applications of acoustic emission monitoring. NDT International. 11: 117–120

ASTM. 1972: Acoustic emission. STP 505

ASTM. 1975: Monitoring structural integrity by acoustic emission. STP 571

Becht, J.; Schwalbe, H. J.; Eisenblaetter, J. 1976: Acoustic emission as an aid for investigating the deformation and fracture of composite materials. Composites. 7: 245–248

Birchon, D. 1975: Non-destructive testing. Engineering design guide, No. 9. Oxford University Press

Bodig, J. 1978: Moisture effects on structural use of wood. Proceedings of symposium: Structural use of wood in adverse environments, Vancouver B.C.

Debaise, G. R.; Porter, A. W.; Pentoney, R. E. 1966: Morphology and mechanics of wood fracture. Mat. Res. Stds. 6: 493–499

Fuwa, M.; Harris, B.; Bunsell, A. R. 1975: Acoustic emission during cyclic loading of carbon-fibre reinforced plastics. J. Phys. D: Appl. Phys. 8: 1460–1471

Fuwa, M.; Bunsell, A. R.; Harris, B. 1976: An evaluation of acoustic emission techniques applied to carbon-fibre composites. J. Phys. D: Appl. Phys. 9: 353–364

Guild, F. J.; Walton, D.; Adams, R. D.; Short, D. 1976: The application of acoustic emission to fibre-reinforced composite materials. Composites 7: 173–179

Harris, D. O.; Tetelman, A. S.; Darwish F. A. 1972: Detection of fibre cracking by acoustic emission. In: ASTM STP 505, 238–249

Kaiser, J. 1950: Untersuchungen über das Auftreten von Geräusch beim Zugversuch. Ph. D. thesis, Technische Hochschule, München

Miller, D. G. 1963: Sounds generated by wood when under stress. Can. Dep. Forest. For. Prod. Res. Bull. Res. News 6: 6–7

Muenow, R. A. 1971: Uses of acoustic emission in construction. Symposium on Acoustic Emission, Bal Harbour, Florida

Muenow, R. A. 1972: Large scale applications of acoustic emission. I.E.E.E. Ultrasonics Symposium, Boston, Mass.

Porter, A. W. 1964: On the mechanics of fracture in wood. Ph. D. Thesis, State Univ. College For., Syracuse University

Porter, A. W.; El-Osta, M. L.; Kusec, D. J. 1972: Prediction of failure of finger joints using acoustic emissions. For. Prod. J. 22: 74–82

Sims, G. D.; Dean, G. D.; Read, B. E.; Western, B. C. 1977: Assessment of damage in GRP laminates by stress wave emission and dynamic mechanical measurements. J. Mat. Sci. 12: 2329–2342

(Received July 24, 1981)

Dr. M. P. Ansell
School of Materials Science
University of Bath
Claverton Down
Bath BA2 7AY
England